Simulation of a Circular Phased Array for a Portable Ultrasonic Polar Scan

Jannes Daemen[1, a)], Mathias Kersemans[2], Arvid Martens[1], Erik Verboven[2], Steven Delrue[1], Wim Van Paepegem[2], Joris Degrieck[2], Koen Van Den Abeele[1]

[1]*Wave Propagation and Signal Processing (WPSP), Department of Physics, KU Leuven-Kulak, 8500 Kortrijk, Belgium*
[2]*Mechanics of Materials and Structures (MMS), Ghent University, Technologiepark-Zwijnaarde 903, 9052 Zwijnaarde, Belgium*

[a)]Corresponding author: jannes.daemen@kuleuven.be

Abstract. The development of new composite materials, often anisotropic in nature, requires intricate approaches to characterize these materials and to detect internal defects. The Ultrasonic Polar Scan (UPS) is able to achieve both goals. During an UPS experiment, a material spot is insonified at several angles $\Psi(\theta,\phi)$, after which the reflected or transmitted signal is recorded. While excellent results have been obtained using an in-house developed 5-axis scanner, UPS measurements with the current set-up are too lengthy and cumbersome for in-situ industrial application. Therefore, we propose to replace the complex mechanical steering of the transducers by a hemispherical phased array consisting of small PZT elements. This allows to create a compact and portable setup without compromising the current data quality. By successively activating a specific set of elements of the array and choosing appropriate inter-element time delays, the beam can be electronically steered from any angle to a fixed position on the targeted sample. Consequently, UPS reflection measurements can be performed at this position from a wide range of angles in a timeframe of seconds. Additionally, by using apodization windows, it is possible to efficiently reduce the intensity of unwanted side lobes and to create a phase profile which closely resembles that of a bounded plane wave, leading to an easier interpretation of the recorded data. The appropriate time delays and apodization parameters can be found though a multi-objective inverse problem in which both the phase profile and the side lobe reduction are optimized. This approach enables the creation of an effective beam profile to be used during UPS experiments for the characterization and inspection of composite materials. Our simulation approach is a crucial step towards a next-generation UPS device for industrial applications and in-field measurements.

Keywords: Ultrasonic Polar Scan, Circular phased array, Bounded plane wave, Genetic Algorithm

INTRODUCTION

The constant need to innovate compels industry to continuously pursue the development of diverse new types of materials. Particularly promising are composite materials such as Carbon Fiber Reinforced Plastics (CFRP). Using the fibers, aligned or arranged in specific orientations, it becomes possible to effectuate a high stiffness-to-weight ratio along these directions. This property is of utmost importance in applications in which weight is a predominant factor with economic importance, such as in airplanes. The downside to this is the introduction of a high degree of anisotropy which makes the mechanical behavior harder to predict. Additionally, as composites are often laminated, they are more prone to internal damage. Thus, the proper behavior of a composite component can only be guaranteed though a good knowledge of its stiffness properties. While several experimental techniques exist to probe the stiffness parameters and to asses internal damage, none of these techniques is all encompassing. For example, the traditional ultrasonic C-scan, well established in the industry, is excellent to uncover material defects[1–3], but fails to provide a quantitative characterization of the target. In contrast, bulk and Lamb wave based techniques do allow for the extraction of stiffness properties in some cases[4,5]. While useful, most of the current approaches require a priori knowledge of the symmetry axes of the composite, which in practice might not always be available.

The Ultrasonic Polar Scan (UPS) was first conceptually conceived in the 1980s[6] and was immediately recognized as a promising characterization tool within the field of NDT. The working principle of the UPS is illustrated in Figure 1(a). A transducer is positioned on a hemisphere at several angles $\Psi(\theta,\phi)$ and generates a quasi-harmonic (H-UPS) signal or broadband pulse (P-UPS) with a center frequency f_c ranging between 1 and 5 MHz. This ultrasonic signal

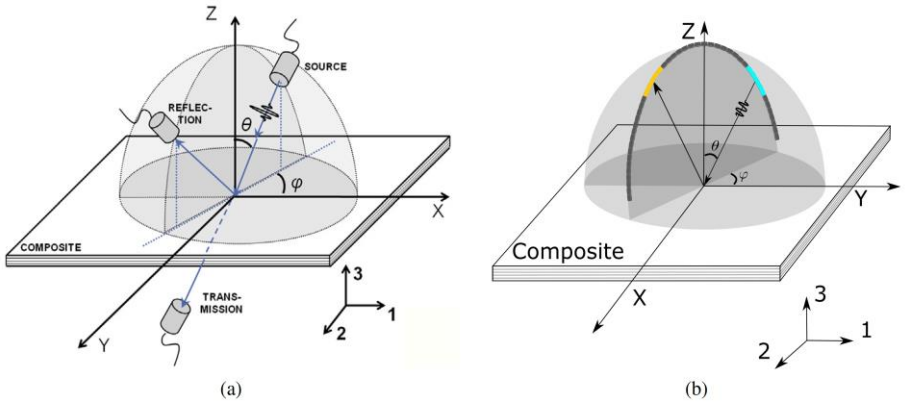

Figure 1. Conceptual drawing of the current UPS setup which is fully water immersed (a) and a handheld UPS device based on a circular phase array (b). Transducer elements highlighted in blue and orange are the emitting and receiving elements respectively.

interacts with the targeted plate and subsequently either the reflection or transmission amplitude and time-of-flight (TOF) is recorded by a receiving transducer. The amplitude or TOF data, sequentially received at a broad range of angles, can be visualized in polar plots in which intriguing patterns emerge. An example of an H-UPS measurement is shown in Figure 2(a). The characteristic features are related to conditions corresponding to an efficient stimulation of Lamb waves[7]. Supplementary, Figure 2(b) shows the result of a P-UPS measurement, in which the contours correspond to the critical bulk wave angles[8]. As both phenomena are strongly related to the unique stiffness parameters of the material, the analysis of the contours provides a viable strategy for characterization. Furthermore, the feasibility of UPS to detect internal damage and (sub)surface corrugation has been demonstrated [9–11].

The UPS results shown in Figures 2(a) and 2(b) were measured with an in-house developed 5-axis scanner in which a single transducer is used to generate the ultrasonic pulse. In a typical UPS measurement, about a million angles $\Psi(\theta, \phi)$ are covered, ensuring a high angular resolution. While excellent results have been obtained using this setup[11], it remains impractical for industrial application. First of all, the setup and the sample must be fully immersed in water to ensure a good coupling between the transducers and the target material. This makes in-situ measurements impossible. Secondly, the positioning of the transducers on the entire hemisphere requires many mechanical movements which might induce additional vibrations and degrade the recorded data quality. Additionally, each angular recording (with θ the scan axis) has to be carried out sequentially, resulting in a relatively long measurement time of about 15 minutes per scan. Thirdly, in the current setup, the receiving transducer adopts a fixed position with respect to the emitting transducer such that only the specular reflection or transmission signal can be recorded. Nonetheless, it has been shown that the non-specular transmission also contains valuable information[12].

In order to tackle the aforementioned problems, a new UPS design is proposed which employs a circular phased array (PA) consisting of small piezoelectric elements. The conceptual design for a circular array is depicted in Figure 1(b). In contrast to mechanical movements, the incident angle θ is now determined by the chosen subset of array elements. Moreover, exploiting the beam steering capabilities of the PA, the incident angle can be supplementary adjusted such that the angular resolution is not limited by the element density of the array. The full electronic control enables the creation of a handheld device which can be used for in-situ measurements and reduces the measurement time drastically, estimated to be in the order of seconds. Furthermore, this arrangement can measure the entire reflection field, i.e. both the specular and non-specular reflection. As such, the additional data could help to improve the extraction of the material properties in an industrial setting. The design of a circular PA is only the first step in the new UPS strategy. For the polar angle dependence, it must be coupled to a one degree of freedom rotation of the circular array. However, a more advanced hemispherical PA would be able to handle this dependence electronically. The full immersion of the setup, required for a proper coupling, can be replaced by a bag of water[13].

Pure bulk and Lamb waves are only produced when an infinite plane wave impinges on a plate[14]. Hence, the characteristic contours observed in the actual UPS measurements, using finite size transducers, do not exactly coincide with the factual appearance of those material waves. Indeed, the integrating effect of the bounded beam produced by a single transducer, which in the far field even appears spherical, does no longer lead to pure modes. Additionally, the main beam is commonly accompanied by side lobes which disturb the measurement. Bearing this in mind, the use of a PA system presents itself with the opportunity to mitigate these problems. By operating the separate elements with

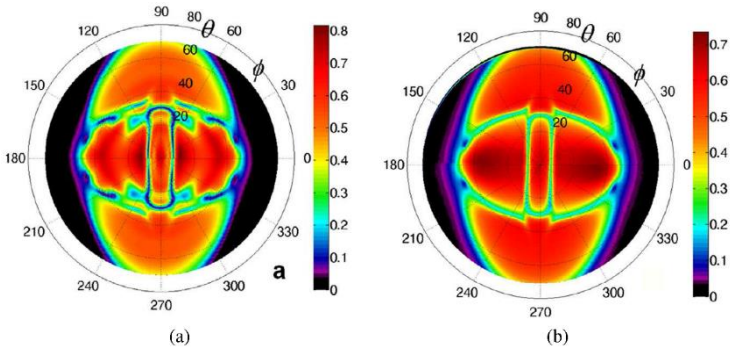

Figure 2. Examples of amplitude polar plots of H-UPS (a) and P-UPS (b) measurements on [0°] carbon/epoxy laminate with a thickness of 1.1 mm and measured at a central frequency f_c = 5 MHz. The extension of the contours along ϕ = 90° is linked to the unidirectional orientation of the carbon fibers in the laminate. Figures are taken from Reference[7].

appropriate phase differences and weighting factors (apodization), the resulting beam can be tuned to reduce the side lobe intensities as much as possible[15,16] and to create a phase profile that maximally resembles a (bounded) plane wave. Especially the latter would eventually simplify the subsequent data analysis as the stimulated waves in the solid will approximate more closely pure bulk and Lamb modes.

In the remainder of this text, the methodology to create a beam with plane wave characteristics and reduced side lobe intensities will be discussed using a simulation approach based on a multiobjective Genetic Algorithm. This constitutes the first crucial step towards the implementation of a real life, handheld UPS device which would be suitable for industrial application.

METHODOLOGY

The elimination of Grating Lobes

In this study, FOCUS has been used to simulate the beam profile of circular arrays characterized by specific sets of phase differences and apodization weights. FOCUS is a Matlab toolbox developed by the Michigan State University[17,18] and allows to define a three-dimensional, arbitrary shaped PA and to calculate the pressure field anywhere in space. This calculation is (semi-)analytical and based on the Spatial Impulse Response of the transducer elements. The underlying theory is essentially an extension of Huygens principle[19]. As such, the time-dependent pressure profile of a single element is expressed as[20]:

$$p(x,y,z;t) = \rho \frac{\partial u(t)}{\partial t} * h(x,y,z;t), \tag{1}$$

where ρ is the medium density, $u(t)$ is the normal velocity of the aperture surface and $h(x,y,z;t)$ is the spatial impulse response function which takes into account the active radiating surface of the aperture. Applying the superposition principle, the sum of the separate pressure contributions then results in the total beam profile. As the calculation is based on an analytical theory, the pressure field computations are fast which is favorable for optimization algorithms. However, the theory assumes that $u(t)$ is uniform across the element aperture, which is unrealistic for PA elements which are bounded near the edges due to gap filling in an attempt to decrease cross-talk effects[21].

The first optimization step consists in determining the appropriate choice of the element size, pitch and array radius to ensure that no grating lobes are produced. Grating lobes are lobes with an intensity similar to the main lobe intensity and are mostly unaffected by apodization. Wooh and Shi have shown that for planar arrays no grating lobes appear as long as the following condition is met[22,23]:

$$d \leq \frac{\lambda}{1+\sin\theta_s}\frac{N-1}{N}, \tag{2}$$

where d is the element pitch, θ_s the steering angle with respect to the normal on the planar array, N the number of activated elements and λ the wavelength. Assuming that θ_s is small and N large, it is clear that the element pitch should not exceed the wavelength. Intuitively, one would expect that this assumption is also valid for the present case of a circular array, as the angle of incidence during a measurement is mainly determined by the element subset and additional steering is minimal. However, it was observed that Equation (2) does no longer strictly hold for a circular

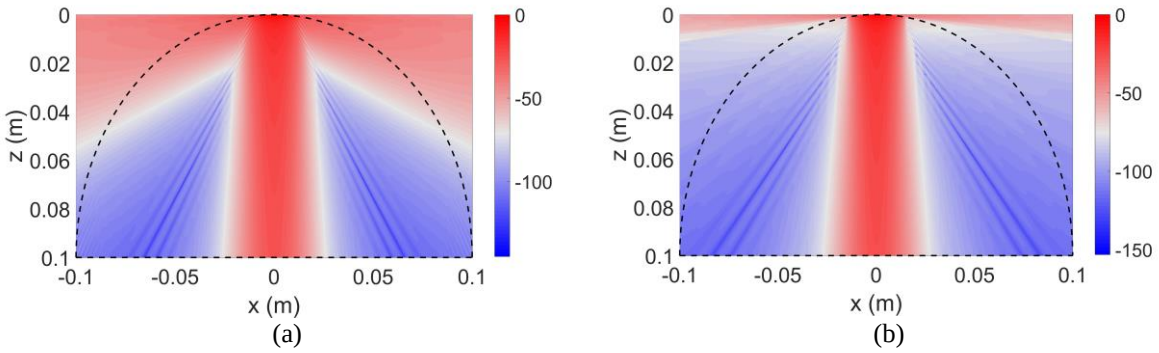

Figure 3. Examples of the influence of the pitch size on the grating lobes for a circular array emitting 1MHz (λ = 1.48 mm) sound waves in water. The color band corresponds to the Sound Press Level (SPL) in dB. The black dashed line denotes the boundaries of the circular array. 35 elements are active with pitch sizes d = 1.4 mm (a) and d = 1.2 mm (b).

array with a finite curvature. An example can be seen in Figure 3(a) for a pitch size of d = 1.4 mm and 35 active elements, with water as the propagation medium and a frequency of 1 MHz (λ = 1.48 mm). It is evident that grating lobes, tilted towards the other array elements, are present. The shape of the array enforces the separate elements to generate a wave at a nonzero incident angle $\theta_n = n\theta_p$ relative to the central element, where n is the element index and θ_p is the angle between two neighboring elements. If it is assumed that the normal to the central element aperture defines the propagation direction of the beam, it can be understood that the full wavefront (of the beam) perpendicular to this direction is steered by an angle θ_n with respect to the nth element. This is schematically shown in Figure 4. Thus, Equation (2) can be rewritten as follows

$$d \leq \lambda \sum_{n=1,2,..,\frac{N-1}{2}} \frac{1}{1+\sin(\theta_n)} \frac{n-1}{n}. \tag{3}$$

In this equation, θ_s and N are replaced by θ_n and n respectively to account of the element specific beam steering. By summing over all elements, the angular effects of each element is incorporated separately. To take into account the symmetry of the system, only integers up to $(N-1)/2$ are included. Note that the effect becomes more severe when more elements are activated or if the curvature increases (θ_n increases). Using equation (3) one finds d = 1.2 mm, which can be used as a first estimation for the pitch. Figure 3(b) shows the beam generated by an array in the same conditions as before, but with a pitch of 1.2 mm. It is clear that grating lobes are now absent. Once the element size, pitch and array radius are chosen according to Equation (3), they are kept fixed in the following optimization step.

Side lobe reduction and the creation of a bounded plane wave

In order to optimize the apodization weights and phase differences between the circular array elements, a multi-objective Genetic Algorithm (GA) has been used in which the intensity and phase profile of each population member considered in the GA is calculated by FOCUS. Furthermore, the GA is implemented in a two-step scheme in which first the apodization weights and subsequently the phase differences are optimized. This leads to a faster convergence. Moreover, in the current case of a circular array, only symmetric solutions are considered useful. Assuming N active elements, this is guaranteed by mirroring the parameters of the first $(N-1)/2$ elements around the central active element, reducing the number of parameters to be optimized to $(N+1)/2$. Additionally, the beam profile, and consequently the fitness functions, only have to be evaluated for positive x-values (lateral direction).

The multiple fitness functions, respectively for phase and intensity profile, to be minimized in the multi-objective GA are defined as follows:

$$f_\phi = \langle|\phi(x)|\rangle \; with \; x \leq l, \tag{4a}$$

$$f_{SPL} = a\sum(M_i - m_i) - \sum(M_i - M_{i+1}), \tag{4b}$$

where, in the first fitness function, $\phi(x)$ denotes the phase at position x on the target evaluation line, and the operation $\langle|\phi(x)|\rangle$ stands for the mean of the absolute value of $\phi(x)$ over a given range. By minimizing the mean of $|\phi(x)|$ for

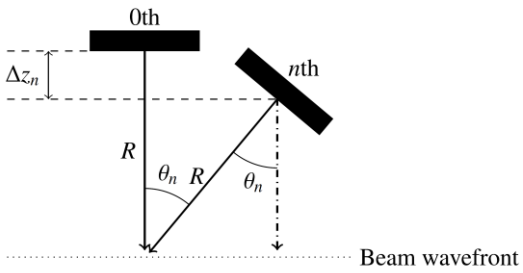

Figure 4. Sketch of the geometry used in the calculation of the pitch condition (Eq. (3)) and the time delays (Eq. (4)). Only the central and the nth element relative to the central element are shown, R, θ_n and Δz_n stand for the radius, angle between the 0th and nth element and the vertical displacement respectively.

x-values between 0 and l (Eq. (4a)), the variation around 0 is limited by the GA, resulting in a bounded plane wave. Whereas larger l-values would result in broader plane waves, which would be beneficial for the excitation of pure Lamb and bulk waves, the minimal variation also typically increases. Therefore, multiple l-values have been tested to find a suitable compromise. In the second equation, a is an arbitrary factor to ensure the second function remains positive, and M_i and m_i denote the ith local maximum and minimum in the intensity profile. The first term of Equation (4b) minimizes the differences between neighboring maxima and minima. As such, a smoother intensity profile is created with less pronounced side lobes. The second term additionally lowers f_{SPL} by favoring large differences between neighboring peaks. This promotes profiles for which each consecutive side lobe is further reduced in intensity, which ensures that the main lobe has a significantly stronger intensity with respect to the background. Note that in contrast to a single-objective GA, a multi-objective procedure does not generate a single best solution. Instead, a set of Pareto optimal solutions is found and manual inspection is required to discern which of these is most suitable[24].

To improve the convergence of the GA, appropriate starting conditions should be considered for the operation parameters. For the apodization weights, classical apodization windows can been considered as these typically reduce the side lobe level[25]. In the current study, we use a Hanning window. The initial phase differences are chosen such that the relative displacement Δz_n of the separate elements is compensated which respect to the central element. Using the geometry shown in Figure 4 and simple trigonometry, the phase difference for the nth element should be $\phi_n = \omega \Delta t_n$, where Δt_n is the time delay given by

$$\Delta t_n = \frac{\Delta z_n}{c_w} = \frac{R(1-\cos\theta_n)}{c_w} \tag{5}$$

In these equations ω, c_w, R and θ_n respectively represent the radial frequency, the speed of sound in water, the radius of the array and the angular position of the element with respect to the central element. Note that - in the two-step optimization - the same initial phase differences have to be used during the optimization of the apodization factors in order capture the basic requirements to create a plane wave.

Finite Elements modeling in COMSOL Multiphysics

In order to assess the quality of the solutions found via FOCUS and the GA, complementary Finite Elements simulations were performed in COMSOL in the frequency domain. The simulated 2D domain for the COMSOL simulations is schematically drawn in Figure 5. Instead of simulating a semicircular domain comprising the entire array, it was opted to truncate the FEM domain, resulting in a lower computation time and memory requirements. In turn, the mesh density can be increased to 20 elements per wavelength such that the accuracy of the results can be guaranteed. A far field calculation[26], starting from the complex pressure values found on the non-reflecting boundaries, is then further used to evaluate the beam profile outside the FEM domain.

The circular PA elements have been modeled as distinct pressure boundaries along the upper arc of the FEM domain with a width and pitch equal to the values used in FOCUS. In contrast to the FOCUS simulations which require a uniform profile over the element aperture, the COMSOL simulations were performed using a non-uniform pressure profile applied to the separate elements, represented by a smoothed block function. This function takes into account the losses near the edges experienced by realistic transducers. On top of these windows, the apodization weights and

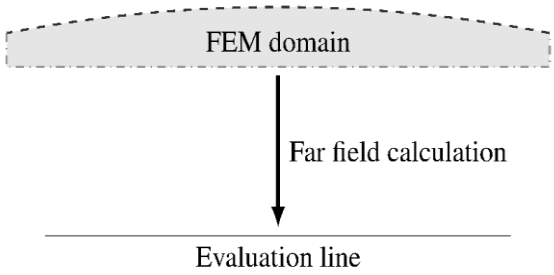

Figure 5. Schematic representation of the truncated 2D FEM model. The black dashed line is a representation of the array elements with predefined size and pitch. The gray dash-dotted line denotes a non-reflecting boundary and demarcates the region of the FEM calculation (gray). The beam profile is calculated on the evaluation/target line by performing a farfield calculation based on the pressure found on the non-reflecting boundaries.

phase differences resulting from the GA optimization are applied to the elements for a comparison with the predictions from FOCUS.

RESULTS AND DISCUSSION

To assess the usefulness of the procedures discussed above, two cases with different element sizes, pitches and operated at different frequencies will be examined. The used parameters can be found in Table 1. The parameters have been deliberately chosen to demonstrate the robustness of the optimization procedure over a broad range of array arrangements and frequencies. The optimized results for both cases have been compared to the beam profiles of non-optimized configurations in which no apodization weights (all constant) and no phase shifts (all zero) are used. In the first case, an additional comparison is made with the pressure field prediction for a single plane transducer that is similar in size to the total width of the activated array elements. To validate the obtained results, the predictions using FOCUS for the optimized parameter set are compared to COMSOL Multiphysics calculations.

Table 1. Specification of the design parameters used in the two case studies. For each case, the width and the pitch (defined as the curved distance between the centers of two neighboring elements) size of the elements were chosen such that no grating lobes are produced. The last column denotes the full size of the active array.

	Width (mm)	Pitch (mm)	Radius (mm)	Frequency (MHz)	Activated Elements (#)	Full size (mm)
Case 1	1	1.1	100	1	39	43.6
Case 2	0.15	0.2	100	5	115	40.3

Case Study 1: 1 MHz

In the first case, we have optimized the apodization and phase differences for a 1 MHz array consisting of 39 elements positioned on an arc of a circle (radius 100 mm) and for an element width of 1 mm with a pitch size of 1.1 mm. Before commenting on the optimized distribution of weight factors and phase differences between the individual elements, let us first discuss the Sound Pressure Level (SPL) and phase profiles resulting from this optimization and their comparison to non-optimized arrangements. The corresponding profiles are visualized in Figures 6(a) and 6(b). A few aspects can be recognized immediately. First of all, the main lobe of the optimized SPL profile is significantly broader than the main lobes of the single transducer (of 43.6 mm width) and of the non-optimized configuration. This was expected, as this is a typical feature of apodized arrays[25]. Especially the main lobe of the non-optimized configuration is very narrow due to the intrinsic focusing behavior of a circular array when no phase differences are applied. Secondly, most side lobes of the optimized result are either eliminated or reduced in intensity with respect to the single transducer solution. Indeed, the only notable peaks in the SPL profile are located at ±23.5 mm and ±32.5 mm with intensities of approximately -21.5 dB and -27.1 dB respectively. Once beyond the second peak, there is a rather smooth decline in intensity, which is in major contrast to the single transducer and to the non-optimized solution. The single transducer simulation result exhibits distinguished side lobes which are typically between 4 and 8 dB stronger with respect to the optimized solution. In addition, the first side lobe is located very close to the main lobe, altering its shape (the farfield has not yet been reached). The SPL profile of the non-optimized arrangement also exhibits a large succession of side lobes which sequentially and rapidly decrease in intensity, for which the levels

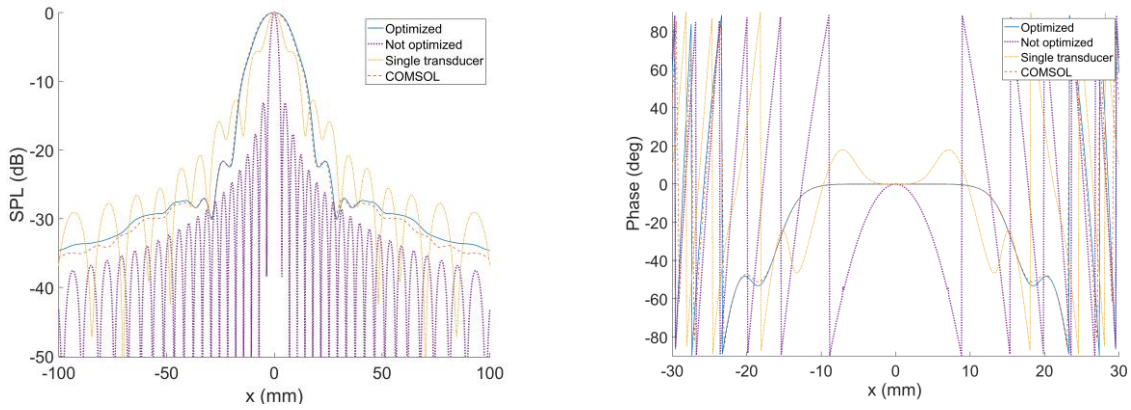

(a) (b)

Figure 6. Optimization results for case 1, showing the SPL profile (a) and the phase profile (b) at the target position, i.e. 100 mm. The full and dotted curves correspond to the optimized and non-optimized configurations respectively. The dash-dotted curve corresponds to a transducer of which the aperture size is comparable to the full activated array size (see Table 1). COMSOL simulations of the optimal configuration are represented by the dashed line.

mostly remain below the SPL of the optimized result. However, its first side lobe is approximately 8 dB stronger and appears much closer to the main lobe compared to the first side lobe of the optimized result. Since the relatively high strength of the first side lobe will be most detrimental to the UPS results, it can be stated that the overall quality of the non-optimized result is worse compared to the optimized result.

The phase profiles in Figure 6(b) also distinctively differ from each other. First of all, the optimized configuration obviously leads to a phase resembling a bounded plane wave. The variations are limited to $2.5 \cdot 10^{-4}$ degrees in a 22 mm wide zone centered around 0. Upon leaving this zone, a rather sharp decrease is observed, which is only disturbed near x = 20 mm due to the presence of the first side lobe. As expected, the non-optimized configuration results in a phase distribution at the evaluation line which is more spherical in nature, owing to the focusing effect of the curved array. Finally, the phase profile of the single plane transducer is approximately flat near the center. However, instead of a smooth decrease, several oscillations are present in the first 20 mm away from the center, corresponding to the position of the first two side lobes. Note that this type of profile is typically observed at the near- to farfield transition. Going deeper into the farfield, the main lobe will become more distinct and generate a phase profile which also resembles a spherical wave. The optimized configuration thus avoids the problem of dealing with the proper interaction distance for single element transducers.

The dashed orange line shown in Figures 6(a) and 6(b) represent respectively the SPL and phase profiles as calculated by COMSOL using the apodization weights and phase differences from the GA optimization. For both profiles, it is clear that the differences between the COMSOL and FOCUS results are minimal, indicating that the results obtained using FOCUS are indeed reliable. It also shows that the simulation procedure as explained above using COMSOL in combination with a far field calculation, works as intended, and that COMSOL Multiphysics will be a valuable tool to model more realistic transducers including the piezo-electric effects.

In order to directly relate the beam quality to the generation of pure wave modes in a plate, it is also interesting to discuss its angular distribution with respect to the central angle of incidence of the beam. The angular distribution is linked to the direction of the various $\boldsymbol{k}(k_x, k_y)$ vectors of which the beam is comprised, expressed by $\vartheta = \sin^{-1}(k_x/|\boldsymbol{k}|)$. Assuming normal incidence, k_x is found by applying a Fourier transform to the complex pressure evaluated at the target position and $|\boldsymbol{k}| = 2\pi/\lambda$. The result of such a calculation for the different arrangements can be seen in Figure 7. The optimized beam profile shows a strong main component at $\vartheta = 0^\circ$, as expected. Due to the boundedness of the beam, the main peak has a non-zero width with a FWHM of about 1.87°, which is reasonably good. Non-negligible contributions at larger angles from 3.5° up to 40° are present, but with much lower intensity (about 22 times smaller than the main component intensity). The beam profile of the single plane transducer also exhibits a clear main component at 0°, although lower in intensity and slightly broader (FWHM ≈ 2.45°). However, the side lobes at higher angles are much more pronounced, reaching relative contributions which are only 5 times smaller than the main component. These contributions definitely distort the generation of pure wave modes in the

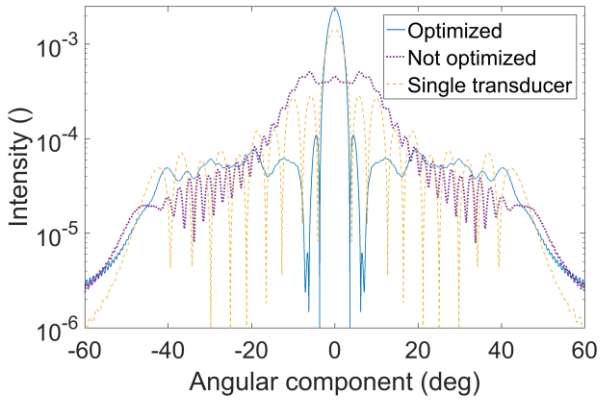

Figure 7. Angular distribution (area normalized to unity) of the beam profiles shown in Figures 6(a) and 6(b). The same color and line types have been used. Notice the logarithmic scale used for the y-axis.

material. Finally, the non-optimized result is no longer dominated by a strong main component. Instead, the main components are found at ±5.95° and the contribution remains large for a wide range of angles (FWHM ≈ 11°). Consequently, standard UPS measurements would be heavily distorted by using this type of beam, possibly exciting multiple neighboring Lamb waves at once.

Having analyzed and discussed the SPL and phase profiles in real and Fourier space, we return to the GA optimized distribution of the apodization weights and phase differences between the elements in the arc of the circular array. Figure 8(a) shows a plot of the 39 optimized apodization weights. Overall, a typical bell-like profile can be seen which is roughly similar to that of traditional apodization windows. Elements positioned far from the center have to be operated at low amplitudes in order to reproduce the desired side lobe reduction. However, whereas one would classically expect the central element to have the highest amplitude, the above discussed 2 step GA optimization procedure advises to drastically lower its value instead. In order to interpret this apodization profile as a whole, one has to consider the phase profile on the evaluation line when a standard apodization window (e.g. Hanning window) is used (and phase shifts of the elements remain unchanged). In such cases, a profile resembling a spherical wave can be observed. This suggest that the apodization weight of the central element primarily influences the phase profile rather than the side lobe reduction, and implies that the phase profile of the central element, spherical in nature due to its small size, dominates the entire profile if its weight is not lowered. In order to get a planar SPL profile, it is thus expected that a GA optimization with a starting condition with a lowered central amplitude will converge faster to a suitable set of parameters. It has been checked that this is indeed the case. Figure 8(b) shows the difference between

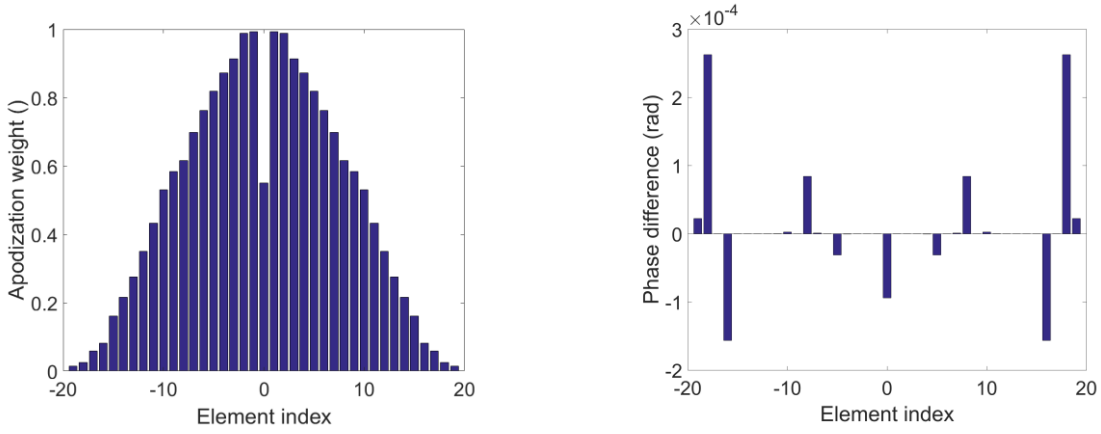

(a) (b)

Figure 8. Distribution of the apodization weights (a) and phase differences with respect to the initial condition, expressed by Equation 4(b) used to generate the optimized beam result shown in Figures 6(a) and 6(b).

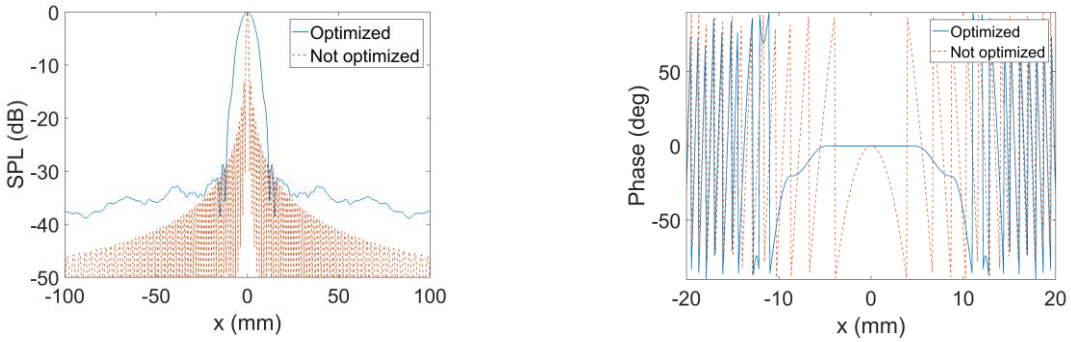

Figure 9. SPL (a) and phase (b) profiles for the optimized and non-optimized configurations for case 2 (5 MHz).

the initially chosen phases as computed by Equation (5) and the optimized set. It can be seen that, overall, the differences are minimal and no systematic pattern can be discerned. This shows that the second optimization step might not be strictly needed and that the strategy to create a plane wave via the initially proposed phase shifts is valid.

Case Study 2: 5 MHz

The second case study concerns the use of a 5 MHz beam created by an circular array (radius 100 mm) with 115 elements with a width of 0.15 mm and a pitch of 0.2 mm, as listed in Table 1. The study is mostly intended to show the robustness of the optimization procedure and therefore the results will not be discussed in as much detail as before. The SPL and phase profiles for both the non-optimized and optimized configuration can be seen in Figures 9(a) and 9(b) respectively. Once more, the SPL profile in the optimized configuration is characterized by a strong main lobe which is quite broad. Furthermore, the first side lobe is found relatively far from the center and is reduced in intensity by about 29 dB. Upon leaving the center, somewhat more variations can be observed compared to the 1 MHz beam discussed above. However, it is still clear that many side lobes have been eliminated compared to the non-optimized solution and that the first side lobe intensity has been drastically decreased. Considering the phase profile, the optimized configuration evidently yields a bounded plane wave, whereas the phase of the non-optimized results again appears more spherical. We noted however that the variation of the phase around the center has increased to the order of $2 \cdot 10^{-2}$ degrees. This is still a reasonable result and together with the proper SPL profile, it can be concluded that the optimization procedure is robust. However, for higher frequencies and smaller elements, the performance of the optimization procedure becomes increasingly harder. This can be attributed to the considerable larger parameter space, the faster variation of the pressure along the beam direction and the increase of the number of side lobes.

To complete this discussion, the optimized apodization parameters used in the second study are plotted in Figure 10. The profile is once again reminiscent of a classical apodization window, but the central weight is lowered. The recurrence of this behavior suggests that the reduced weight in the central element is the most important feature to create the bounded plane wave using a circular array, and that it is not dependent on the element and pitch sizes of the array.

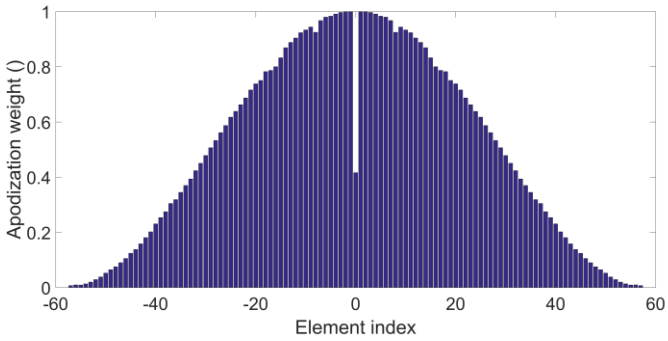

Figure 10. Distribution of the apodization weights in order to produce the results in figures 9(a) and 9(b).

CONCLUSION

In this work, the first step towards a handheld UPS device, namely the creation of a suitable planar beam using a circular PA, has been discussed. A two-step optimization scheme has been presented based on a multi-objective Genetic Algorithm (GA) to find the appropriate apodization weights and phase differences for the elements in the array for which the resulting beam has a maximally extended planar profile with a minimal intensity in the side lobes. FOCUS, a Matlab toolbox based on the Impulse Response Function, was used to calculate the beam profile for each population member (representing a set of apodization and phase parameters) considered in the GA. The procedure has been illustrated and discussed for two test cases (1 and 5 MHz). In each case, beam profiles with drastically reduced side lobe levels and a phase resembling a bounded plane wave have been successfully obtained using a distribution of apodization weights reminiscent of classical apodization windows, but with a lowered central weight. This suggests that the central apodization weight is a key player in the creation of a bounded plane wave with a circular PA. It was also observed that starting from geometry based initial conditions, a further optimization of the elementwise phase shifts is not strictly needed. The two different configurations have shown the robustness of the technique, although it is also clear that for a larger parameter space (i.e. more elements) and high frequencies, good results are attained with more difficulty.

ACKNOWLEDGMENTS

Support from the Fund for Scientific Research-Flanders (FWO Vlaanderen, grant G0B9515N) is gratefully acknowledged.

BIBLIOGRAPHY

[1] C.C. Tsao and H. Hocheng, Int. J. Mach. Tools Manuf. **44**, 1085 (2004).
[2] K. Imielińska, M. Castaings, R. Wojtyra, J. Haras, E.L. Clezio, and B. Hosten, J. Mater. Process. Technol. **157**, 513 (2004).
[3] Y.O. Kas and C. Kaynak, Polym. Test. **24**, 114 (2005).
[4] S. Siva Shashidhara Reddy, K. Balasubramaniam, C.V. Krishnamurthy, and M. Shankar, Compos. Struct. **67**, 3 (2005).
[5] A.H. Nayfeh and D.E. Chimenti, J. Appl. Mech. **55**, 863 (1988).
[6] V. DREUMEL, Mater. Eval. **39**, 922 (1981).
[7] M. Kersemans, A. Martens, K. Van Den Abeele, J. Degrieck, L. Pyl, F. Zastavnik, H. Sol, and W. Van Paepegem, Ultrasonics **58**, 111 (2015).
[8] M. Kersemans, N. Lammens, J. Degrieck, K. Van Den Abeele, L. Pyl, F. Zastavnik, H. Sol, and W. Van Paepegem, Wave Motion **51**, 1071 (2014).
[9] M. Kersemans, A. Martens, K.V.D. Abeele, J. Degrieck, F. Zastavnik, L. Pyl, H. Sol, and W.V. Paepegem, J. Nondestruct. Eval. **33**, 522 (2014).
[10] M. Kersemans, I. De Baere, J. Degrieck, K. Van Den Abeele, L. Pyl, F. Zastavnik, H. Sol, and W. Van Paepegem, Polym. Test. **34**, 85 (2014).
[11] M. Kersemans, A. Martens, J. Degrieck, K. Van Den Abeele, S. Delrue, L. Pyl, F. Zastavnik, H. Sol, and W. Van Paepegem, Appl. Sci. **6**, 58 (2016).
[12] M. Kersemans, Combined Experimental-Numerical Study to the Ultrasonic Polar Scan for Inspection and Characterization of (Damaged) Anisotropic Materials, Universiteit Gent, 2014.
[13] J. Camacho, J.F. Cruza, J. Brizuela, and C. Fritsch, IEEE Trans. Ultrason. Ferroelectr. Freq. Control **61**, 673 (2014).
[14] A.H. Nayfeh, *Wave Propagation in Layered Anisotropic Media: With Application to Composites* (Elsevier, 1995).
[15] A. McNab, A. Cochran, and M.A. Campbell, J. Acoust. Soc. Am. **87**, 1455 (1990).
[16] D.A. Guenther and W.F. Walker, IEEE Trans. Ultrason. Ferroelectr. Freq. Control **54**, 343 (2007).
[17] R.J. McGough, J. Acoust. Soc. Am. **115**, 1934 (2004).
[18] R.J. McGough, T.V. Samulski, and J.F. Kelly, J. Acoust. Soc. Am. **115**, 1942 (2004).
[19] P.R. Stepanishen, J. Acoust. Soc. Am. **49**, 841 (1971).
[20] C. Zou, Z. Sun, D. Cai, S. Muhammad, W. Zhang, and Q. Chen, Sensors **16**, 1873 (2016).
[21] B.W. Drinkwater and P.D. Wilcox, NDT E Int. **39**, 525 (2006).
[22] S.-C. Wooh and Y. Shi, Ultrasonics **36**, 737 (1998).
[23] S.-C. Wooh and Y. Shi, Wave Motion **29**, 245 (1999).
[24] J. Branke, K. Deb, and K. Miettinen, *Multiobjective Optimization: Interactive and Evolutionary Approaches* (Springer Science & Business Media, 2008).
[25] L.W. Schmerr Jr., *Fundamentals of Ultrasonic Phased Arrays* (Springer, 2014).
[26] COMSOL Multiphysics 5.3, in *Acoust. Module User Guide* (2017).